


# Investigating the Influence of Desulfurization Fly Ash on the Upgrading of Biomass-Derived Pyrolysis Gas

Ranyilong You, Xinyu Yang, Chuyang Tang ,\* and Xinyang Zhou

The catalytic role of desulfurization fly ash (DFA) was explored as a means to upgrade biomass-derived pyrolysis gas, with a focus on integrating waste valorization and renewable energy production. Soybean straw (SS) was pyrolyzed with DFA to assess the influence on pyrolytic product distribution. The results indicate that DFA notably influenced the yield and quality of pyrolysis gas, with optimal yields achieved at specific DFA concentrations. The study also demonstrated that DFA enhanced the production of methane (CH<sub>4</sub>) and hydrogen (H<sub>2</sub>) while reducing carbon monoxide (CO), thereby improving the lower heating value of pyrolysis gas. Fourier-transform infrared (FT-IR) spectroscopy and scanning electron microscopy (SEM) were employed to characterize the char, showing increased surface area and pore volume due to DFA addition. The study concluded that DFA is an effective catalyst in biomass gasification, providing valuable insights into its catalytic mechanisms and potential for industrial application.

DOI: 10.15376/biores.20.2.2544-2555

Keywords: Desulfurization fly ash; Soybean straw; Catalytic pyrolysis; Pyrolysis gas

Contact information: School of Civil Engineering, University of Science and Technology Liaoning, 189#, Qianshan Road, Liaoning Province 114051, PR China; \*Corresponding author: astcy@ustl.edu.cn

## INTRODUCTION

In the manufacturing sector, operations such as phosphate ore processing, kerosene combustion, and aluminum smelting, in addition to volcanic activity, result in the release of flue gases that are rich in sulfur dioxide (Peng *et al.* 2024). This gas is highly irritating to the respiratory system. Once inhaled, it can lead to the formation of corrosive compounds, including sulfurous acid, sulfuric acid, and sulfates, which accumulate in the moist linings of the airways. These compounds have significant detrimental effects on human health (Chen *et al.* 2007). In the past few decades, semi-dry flue gas desulfurization technology has advanced significantly due to its superior efficiency and economic viability, particularly in regions such as the European Union and China (Li *et al.* 2019). Desulfurization fly ash (DFA), a byproduct of the flue gas desulfurization process, has emerged as a potential resource for various applications, owing to its high calcium content and alkalinity (Ning *et al.* 2025). The estimated global production of desulfurization fly ash in 2023 is approximately 1.63 billion tons. However, the usage of DFA remains limited due to its high moisture content, poor stability, and potential environmental risks particularly from heavy metal leaching (Wang *et al.* 2021). Currently, DFA is primarily used as a soil amendment or in the production of construction materials, due to its beneficial effects on soil structure and nutrient availability (Li *et al.* 2022b; Ma *et al.* 2022). Nonetheless, these applications have been constrained by the high transportation costs and the need for pretreatment to mitigate environmental risks.

In contrast, biomass, as a renewable energy source, has been increasingly utilized to produce biofuels and chemicals (Mohan *et al.* 2024). Most biomass is derived from agricultural residues and forestry waste, yet it remains underutilized despite its significant potential for energy production and environmental benefits (She *et al.* 2024). The challenges in biomass utilization include the variability in feedstock quality, the need for efficient pretreatment methods, and the economic viability of conversion processes (Sun *et al.* 2024). Generally, pyrolysis gas derived from biomass pyrolysis tends to have a high oxygen content and low calorific value (Xie *et al.* 2012; Ren *et al.* 2013). The development of cost-effective and environmentally sustainable technologies for biomass conversion is essential to overcome these hurdles and to realize the full potential of biomass as a renewable resource (Mlonka-Mędrala *et al.* 2021). However, biomass conversion into pyrolysis gas, a key intermediate, is often energy-intensive and faces challenges, such as tar formation and catalyst deactivation (Wang *et al.* 2024). Utilizing catalysts to regulate the pyrolysis of biomass has been shown to be an effective method for enhancing the quality of pyrolysis products (Zhang *et al.* 2025). Recent literatures revealed that calcium-based compounds can effectively catalyze the biomass pyrolysis, enhancing the yield and quality of the pyrolysis gas produced (Mariyam *et al.* 2024; Zhang *et al.* 2024). The main components of DFA are calcium sulfite and calcium hydroxide (Ruan *et al.* 2023). Therefore, the direct application of DFA in biomass gasification could circumvent these issues by utilizing the material *in situ*, thereby reducing costs and environmental impacts (Zhou *et al.* 2024). Moreover, the integration of DFA with biomass conversion processes presents a dual advantage: it allows for the valorization of a waste material while enhancing the efficiency of biomass gasification. A comprehensive understanding of the catalytic mechanisms involved is necessary to fully exploit the potential of DFA in this context. The utilization of DFA in upgrading biomass pyrolysis gas is a promising avenue for waste valorization and renewable energy production. The successful experimental study of DFA as a catalyst or catalyst support in biomass gasification will offer a method to promote the biomass conversion to pyrolysis gas by the resource application of industrial solid waste. However, the underlying catalytic mechanisms of DFA in biomass pyrolysis gas upgrading remain unclear, which is critical for optimizing its application and realizing its full potential.

This study aimed to fill the knowledge gap by investigating the catalytic role of DFA in the upgrading of biomass-derived pyrolysis gas, addressing both the current limitations and the prospects of this integrated approach. Herein, DFA was employed to investigate the catalytic pyrolysis of SS at temperatures below 600 °C. Pyrolysis experiments were conducted to evaluate how DFA additives influence the distribution of pyrolysis products. Additionally, the catalytic mechanism of DFA was analyzed with respect to both the yield and characteristic of pyrolysis gas and char generated from SS pyrolysis by utilizing model compounds.

## EXPERIMENTAL

### Raw Materials and Process of Pyrolysis

In this study, desulfurization fly ash (DFA) was obtained from the Anshan Steel II power plant, while soybean straw (SS) was collected from rural areas in Liaoning province. Both DFA and SS samples were dried at 105 °C for 8 h, then ground to achieve particle sizes below 0.178 mm. Elemental composition was assessed using a Macro Cube analyzer

from Elementar, located in Berlin, Germany. The detailed proximate and ultimate analysis results for SS are presented in Table 1.

**Table 1.** Proximate and Ultimate Analysis of SS

Proximate Analysis (wt%)		Ultimate Analysis (wt%, daf)	
Moisture (ad <sup>a</sup> )	6.67	Carbon (C)	45.54
Ash (d <sup>d</sup> )	1.96	Hydrogen (H)	6.79
Volatile Matter (daf <sup>a</sup> )	84.50	Nitrogen (N)	1.28
CS (daf)	15.50	Sulfur (S)	0.33
--	--	Oxygen (O) (diff <sup>b</sup> )	46.06

<sup>a</sup> ad, air-dried benchmark; <sup>d</sup> d, dry benchmark; daf, dry and ash-free benchmark;  
<sup>b</sup> Calculated by difference

The crystal structure of DFA was elucidated using X-ray diffraction (XRD) on a D8-ADVANCE instrument from Bruker, Germany. The XRD measurements covered a  $2^\circ$  to  $80^\circ$   $2\theta$  range with a resolution of  $0.0001^\circ$ .

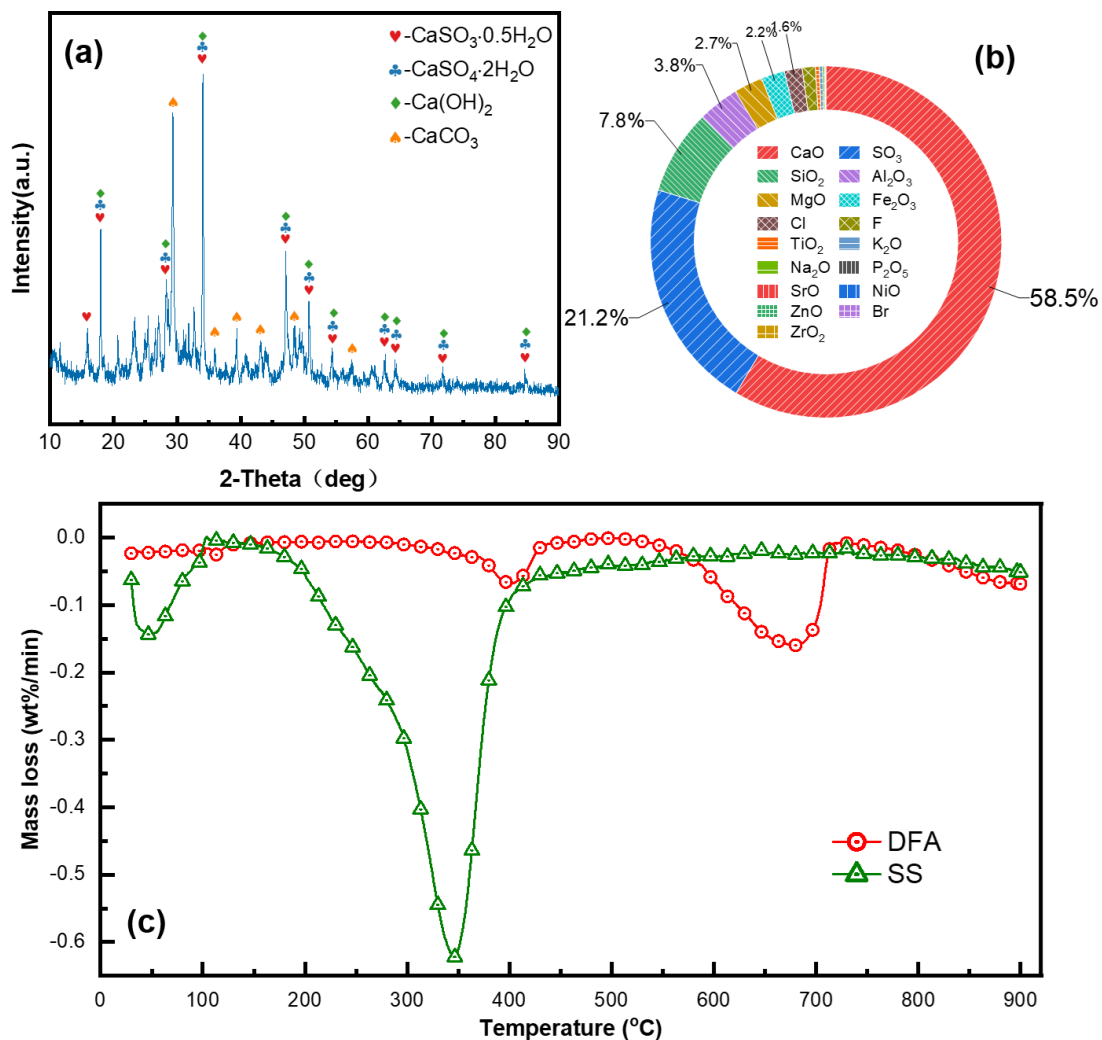


**Fig. 1.** Characteristics of DFA and SS: (a) XRD analysis of DFA; (b) XRF result of DFA; (c) DTG curves of DFA and SS

Elemental composition of the DFA was determined by XRF spectroscopy using an S8TLGER analyzer, also from Bruker, Germany. The corresponding XRF data are shown in Fig. 1(b). Thermogravimetric analysis (TGA) was employed to evaluate the thermal stability of the sample, conducted on a TG-DTA/DSC instrument from Bruker, Germany. Approximately 30 mg of each sample was heated from ambient temperature to 900 °C at a rate of 5 °C/min under a nitrogen atmosphere, with a gas flow rate of 20 mL/min to protect oxidation. The thermal decomposition profiles are illustrated in Fig. 1(c).

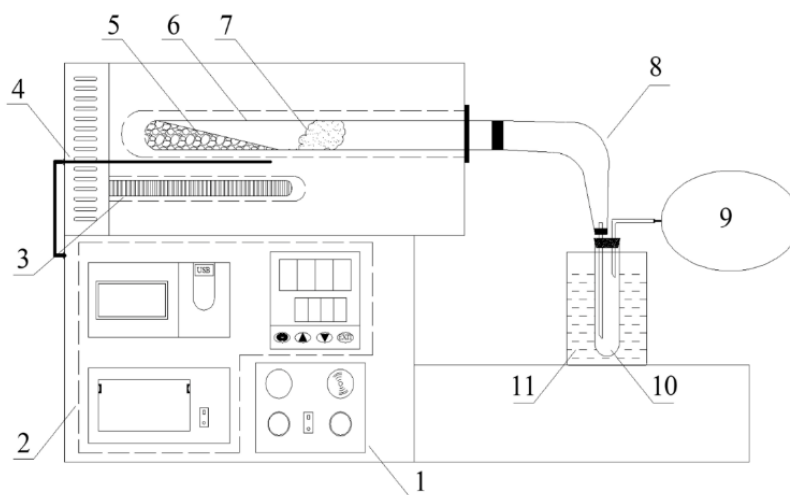


**Fig. 2.** Schematic diagram of the pyrolysis apparatus: 1. heating control; 2. temperature regulation; 3. bolt electric heaters; 4. thermocouple; 5. samples; 6. tubular reactor; 7. asbestos wool; 8. plain bend; 9. gas bag; 10. condenser; 11. ice bath

As part of the catalytic pyrolysis study, experiments involving SS and DFA were conducted within a tube furnace, following the setup depicted in Fig. 2 and the methodology outlined in a previous publication by the authors (Tang *et al.* 2015). The test samples consisted of SS and DFA blended in a specific mass ratio. Approximately 4 g of this mixture was measured and introduced into a quartz tube reactor. The samples were heated from ambient temperature to 600 °C at a rate of 5 °C/min, followed by a 15-min dwell at this temperature. After the experiment, the weight of the reaction tube and the liquid phase condensation collector was measured to determine the mass difference, which was used to calculate the yields of char and liquid phase products. The water yield was determined using the toluene-assisted method (ASTM D4006-11 2012). Pyrolysis gas was captured in a gas bag, and its volume was measured using the water displacement technique.

## Methods

### *GC analyses of pyrolysis gas*

The composition of the pyrolysis gas was analyzed using a GC 126 gas chromatograph (INESA Instrument Co., Shanghai, China), equipped with both a flame ionization detector and a thermal conductivity detector. The gas sample, obtained from the pyrolysis experiment, was introduced to the GC 126 at a flow rate of 30 to 50 mL/min for the quantification of its primary constituents: hydrogen (H<sub>2</sub>), methane (CH<sub>4</sub>), carbon monoxide (CO), and carbon dioxide (CO<sub>2</sub>).

### Characterization of char

Fourier transform infrared (FT-IR) spectroscopy was conducted using a VERTEX-70 Spectrophotometer to characterize the functional groups within the frequency range of 400 to 4000  $\text{cm}^{-1}$  at a resolution of 4.0  $\text{cm}^{-1}$ . The surface morphology of the char was examined using a Thermo Fisher Apreo 2 scanning electron microscope (SEM). Nitrogen adsorption isotherms for the char were determined with a Micromeritics APSP 2460 analyzer, employing the Brunauer-Emmett-Teller method (BET) and Barrett-Joiner-Halenda method (BJH).

## RESULTS AND DISCUSSION

### Characteristics and DTG Analysis of DFA and SS

As shown in Table 1, the SS sample exhibited a high volatile matter content of 84.50 wt%, while its ash content was relatively low, amounting to only 1.96 wt%. The diffraction patterns, depicted in Fig. 1(a), revealed the presence of  $\text{CaSO}_3 \cdot 0.5\text{H}_2\text{O}$ ,  $\text{CaSO}_4 \cdot 2\text{H}_2\text{O}$ ,  $\text{Ca}(\text{OH})_2$ , and  $\text{CaCO}_3$  in the DFA sample, as shown in Fig. 1 (a) and (b). Moreover, the  $\text{CaSO}_3$  content in DFA was quantified at 31.9 wt% through XRD and X-ray fluorescence (XRF) analyses. The cellulose and lignin contents in SS were determined as 30.8% and 32.8% respectively, using the analytical method described by David Díez *et al.* (2020). For the pyrolysis experiments, microcrystalline cellulose (MCC) and dealkali lignin (LG) were served as model compound.

As illustrated in Fig. 1(c), the thermal decomposition of SS occurred in three stages. The first stage, the drying phase (from room temperature to 150 °C), involved the removal of free water and degassing, resulting in a total mass loss of 8.28 wt%. The second stage the main thermal decomposition phase (150 °C to 420 °C), consisted of two periods: the pre-pyrolysis phase and the rapid pyrolysis phase. In the initial phase (140 to 280 °C), the rate of thermal weight loss increased rapidly as cellulose and hemicellulose in SS underwent depolymerization and ring-opening reactions (Bassilakis *et al.* 2001). Additionally, the carboxyl functional groups in lignin and cellulose underwent C-O bond cleavage, releasing hydroxyl radicals, while some methoxy side chains on the cellulose also were broken, releasing methoxy radicals (Yao *et al.* 2019). When the temperature exceeded 280 °C, the rate of thermal weight loss of SS gradually decreases. At this point, the large aggregate structures in SS had been destroyed, and the bridges between cellulose structural units also broke, releasing many alkyl radicals. The peak thermal weight loss range for SS was between 280 and 420 °C, with the maximum rate of thermal weight loss at 0.623 wt%/min, which is the primary stage for pyrolysis gas and tar formation. The third stage was the char formation phase (> 420 °C), during which the aromatic structures in the straw began to condense, increasing the aromaticity of the pyrolysis residues, while hydrogen and carbon monoxide were released. Due to the influence of weight loss and temperature, the rate of mass loss of SS samples slowed down in this stage. When the temperature exceeded 550 °C, the process entered the pyrolytic condensation stage, where the rate of thermal weight loss stabilized. The stabilization of the mass indicated that the thermal decomposition reaction was essentially complete, resulting in the formation of char.

The DTG curve of DFA exhibited four weight loss stages. In the first stage (< 200 °C), free water was released from DFA, and  $\text{CaSO}_3 \cdot 0.5\text{H}_2\text{O}$  underwent dehydration, removing crystalline water, resulting in a weight loss of 2.5 wt%. The second stage (200

to 500 °C) was characterized by a weight reduction of approximately 7.5 wt%. Combined with XRD analysis, this loss can be primarily attributed to the decomposition reaction of  $\text{Ca}(\text{OH})_2$ . The maximum thermal weight loss rate occurred at 400 °C, at 0.067 wt%/min. The third stage spanned from 500 to 720 °C, with the maximum thermal weight loss rate occurring at 670 °C (0.162 wt%/min). This weight loss is primarily due to the thermal decomposition of  $\text{CaCO}_3$ , releasing  $\text{CO}_2$ . In the fourth stage ( $\geq 720$  °C), DFA enters pyrolysis, with weight loss mainly attributed to the decomposition of  $\text{CaSO}_3$ , releasing  $\text{SO}_2$ .

### Influence of DFA on Pyrolysis Product Yields

Figure 3(a) illustrates the distribution of yields from the pyrolysis products of DFA/SS. As the DFA content in the sample increased, the yield of char also increased. The yield of pyrolysis gas initially increased and then decreased with increasing DFA content, peaking at 33.3 wt% DFA, where the yield reached 27.3 wt%.

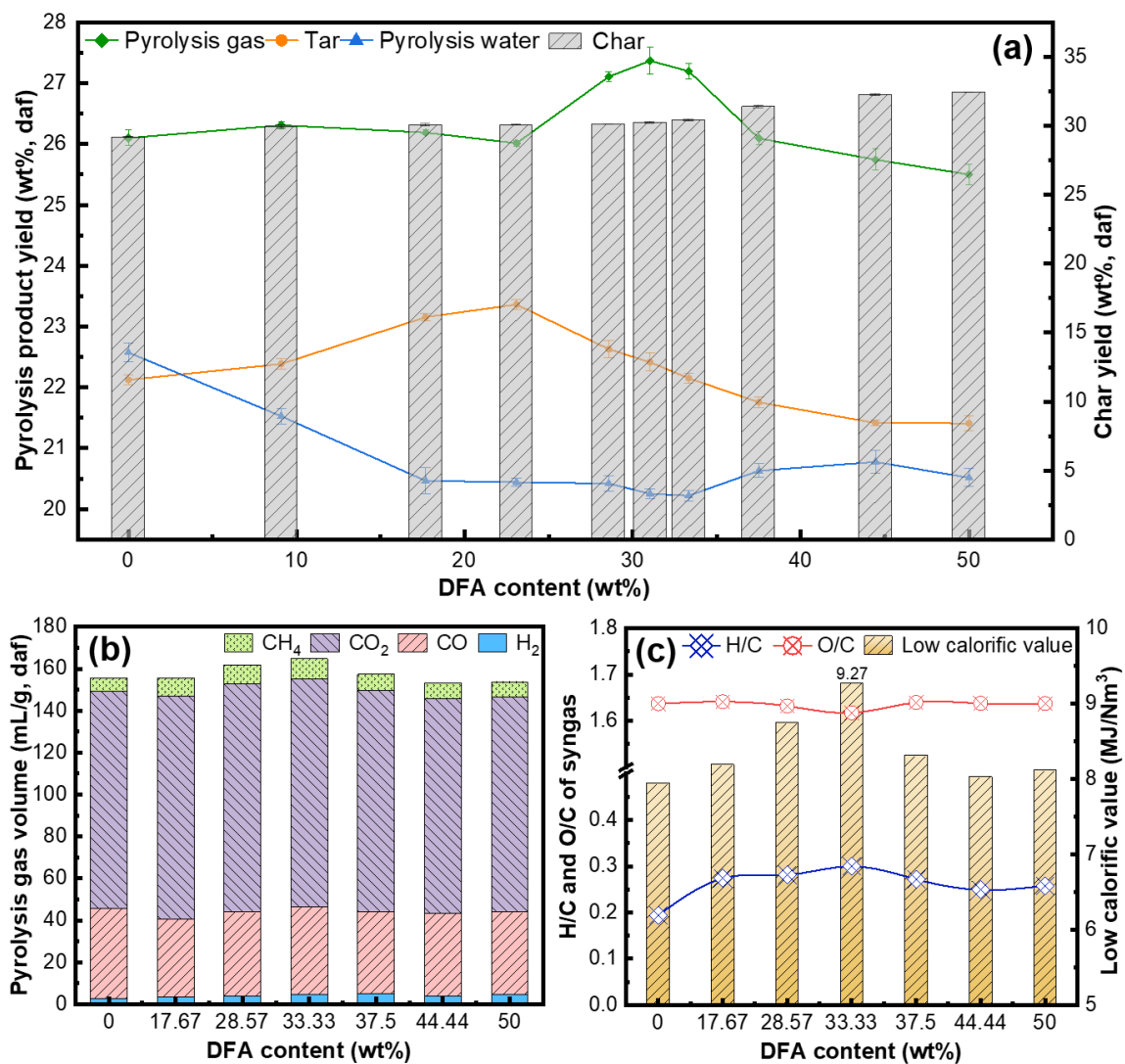


**Fig. 3.** DFA effects on the yield characteristics of catalytic pyrolysis products: (a) DFA impact on the yield of pyrolysis products; (b) GC results of pyrolysis gas; (c) Characteristics of pyrolysis gas

Similarly, the yield of tar exhibited a trend similar to that of pyrolysis gas, with the maximum yield of 23.1 wt% (daf) corresponding to a DFA content of 23.4 wt% in the sample. Conversely, the yield of pyrolysis water decreased initially and then increased with the addition of DFA, reaching its minimum of 20.3 wt% (daf) at a DFA content of 33.3 wt%. These results indicate that DFA had distinct catalytic effects on the formation of different pyrolysis products from SS. Within a certain range of DFA/SS ratio, DFA remarkably promoted the decomposition of SS to generate pyrolysis gas and tar, while inhibiting the production of pyrolysis water.

As shown in Fig. 3(b), GC results demonstrated that DFA significantly affected the composition and volume of pyrolysis gas. DFA catalyzed the pyrolysis of SS, resulting in an increased pyrolysis gas yield. The maximum pyrolysis gas volume (165 mL/g) occurred at 33.3 wt% DFA, representing a 6.0% increase compared to the pyrolysis of SS alone. The peak volumes of CH<sub>4</sub>, CO, and CO<sub>2</sub> were 9.67 mg/L, 41.90 mg/L, and 108.54 mL/g, respectively, at 33.3 wt% DFA. The DFA enhanced CH<sub>4</sub> generation, with the CH<sub>4</sub> yield from DFA/SS pyrolysis being 48.9% higher than that from SS pyrolysis alone. Conversely, DFA reduced the production of CO, with the maximum CO yield from the pyrolysis of DFA/SS being only 96.9% of that from the pyrolysis of SS alone. The catalytic effect of DFA significantly boosted H<sub>2</sub>. At 37.5 wt% DFA, the H<sub>2</sub> yield from DFA/SS pyrolysis reached 4.65 mL/g, which was 1.75 times that of SS pyrolysis. Moreover, DFA's catalytic effect increased CH<sub>4</sub> and H<sub>2</sub> production in SS pyrolysis gas, thus enhancing the lower heating value (LHV) of DFA/SS pyrolysis gas. As shown in Fig. 3(c), the maximum lower heating value of DFA/SS pyrolysis was 9.27 MJ/m<sup>3</sup>, which was 16.8% more than that of SS pyrolysis alone. Furthermore, the H/C at a 33.3 wt% DFA was 1.58 times that of SS pyrolysis alone due to the increased production of CH<sub>4</sub> and H<sub>2</sub>, and decreased production of CO in the pyrolysis gas of DFA/SS. While the content of DFA was 33.3%, the O/C ratio of the DFA/SS pyrolysis gas was 1.62, which was lower than that of the SS pyrolysis alone. This indicates that DFA improved the quality and volume of the pyrolysis gas from DFA/SS pyrolysis.

### Morphology and Characterization of Char

Figure 4 presents the surface morphological analysis of DFA/SS char and SS char. Examination of Fig. 4(a), (b), and (c) reveals that the surface of SS char was characterized by densely packed, bundled structures, which were notably lacking porosity. The char exhibited relatively sheet-like structures and with cracks induced by heating. Additionally, Fig. 4(c) shows that the residual vascular structures on the char surface contain numerous small pores. This phenomenon can be attributed to the decomposition and condensation of lignin and cellulose during SS pyrolysis, which exposes the vascular bundles within the straw.

The DFA/SS char exhibited a more irregular surface with wrinkles and crevices. Moreover, their sheet-like structure was disrupted and covered with spherical particles. This indicates that DFA facilitated the thermal decomposition of SS. As evident in Fig. 4(e), the sheet-like structure of DFA/SS char was disrupted, leading to the emergence of micro-scale holes, which suggests an increased specific surface area. Figure 4(f) reveals that these spherical particles displayed distinct crystalline cluster-like structures with numerous micropores on their surfaces. This suggests that they are calcium salt particles formed after the loss of crystalline water from DFA upon heating. Overall, the interaction between DFA and SS during the pyrolysis process resulted in the formation of numerous slits and micropores on the surface of the DFA/SS char.

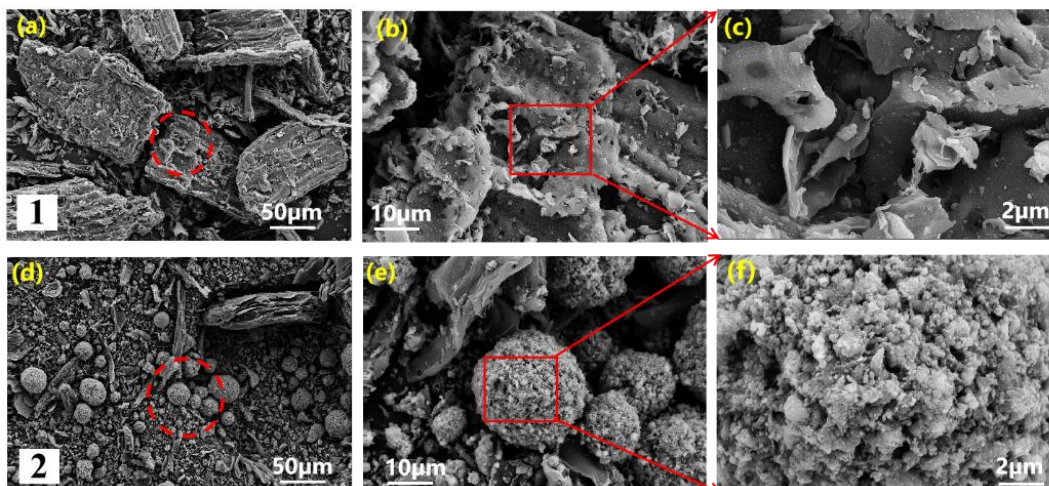


**Fig. 4.** SEM images of SS and DFA/SS char: (a), (b), (c) Surface topography of SS char; (d), (e), (f) Surface topography of DFA/SS char

Figure 5(a) displays the Fourier-transform infrared (FT-IR) spectra of SS and DFA/SS char, which provide insights into the chemical composition of the char surface post-pyrolysis, as determined by FT-IR analysis. As the DFA content increases, important shifts and intensifications in the absorption bands are observed. A minor peak around  $3400\text{ cm}^{-1}$  corresponds to the  $-\text{OH}$  group. With increasing DFA content, the abundance of the  $-\text{OH}$  group decreased, suggesting that the catalytic action of DFA facilitated the cleavage of  $-\text{OH}$  in SS. The peak at  $1650\text{ cm}^{-1}$  is indicative of the  $\text{C}=\text{O}$  group. Compared to the SS char, the  $\text{C}=\text{O}$  peak on the DFA/SS char surface was moderately intensified, suggesting that DFA addition catalyzed the cleavage of  $-\text{COOH}$  and  $-\text{C}-\text{O}-$  in SS. The heightened  $\text{C}=\text{O}$  peak may signal dehydration reactions or the decomposition of carbonyl-containing compounds, potentially affecting the reactivity and applications of the resultant char material. The bands associated with  $\text{Ca}(\text{OH})_2$  ( $1800\text{ cm}^{-1}$ ),  $\text{CaCO}_3$  ( $1440\text{ cm}^{-1}$ ),  $\text{CaSO}_4$  ( $1150\text{ cm}^{-1}$ ), and  $\text{CaSO}_3$  ( $875\text{ cm}^{-1}$ ) showed a notable increase in intensity with higher DFA content. However, the rise in calcium hydroxide's abundance was minimal, implying that  $\text{Ca}(\text{OH})_2$  reacted with  $\text{CO}_2$  emanating from SS decomposition to form  $\text{CaCO}_3$  during the DFA/SS pyrolysis. This reaction may enhance the calorific value of the DFA/SS pyrolysis gas to some extent.

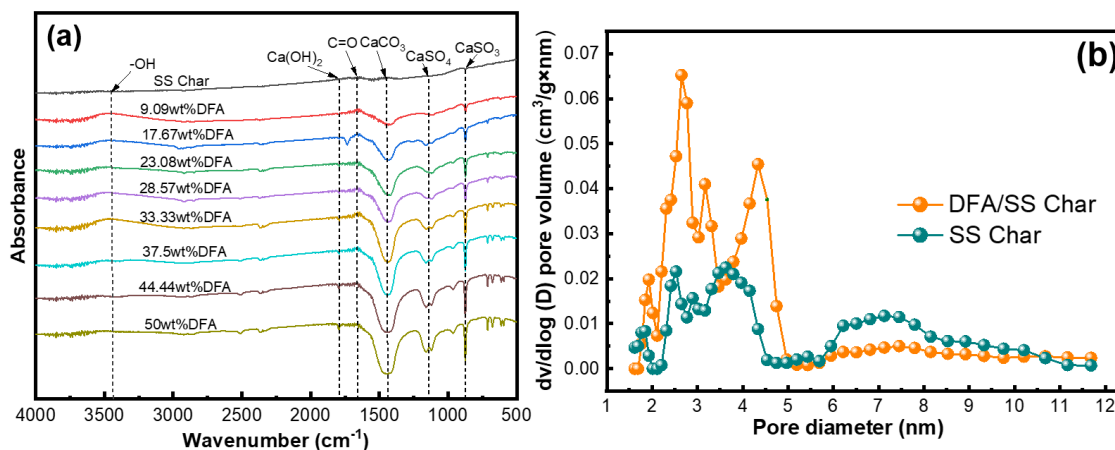


**Fig. 5.** Characteristics of SS and DFA/SS char: (a) FT-IR curves of SS and DFA/SS char; (b) The BET-BJH analysis of SS and DFA/SS char



Further analysis of pore size distribution for SS and DFA/SS char is presented in Fig. 5(b). The specific surface area of DFA/SS char was  $12.2 \text{ m}^2/\text{g}$ , which was significantly higher than that of SS char, which was  $6.24 \text{ m}^2/\text{g}$ . Moreover, the total pore volume of DFA/SS char was  $0.0209 \text{ cm}^3/\text{g}$ , representing a 23.7% increase compared to SS char. Notably, the micropore specific surface area of DFA/SS char was 2.44 times greater than that of SS char. The presence of DFA significantly enhances the decomposition of SS. Compared to SS pyrolysis alone, DFA catalytically promoted the formation of more crevices and pore structures on the surface of SS char during DFA/SS pyrolysis.

### Investigating Pyrolysis Mechanisms *via* Model Compounds

As previously discussed, the addition of DFA markedly increased the yield of  $\text{CH}_4$  and  $\text{H}_2$  during the pyrolysis of DFA/SS. To further investigate the catalytic influence of DFA on the various constituents of SS, a model compound approach was employed. Specifically, microcrystalline cellulose (CE) and alkaline lignin (LG) were chosen as representative model compounds. Accordingly, the DFA content in the blends of DFA/CE was adjusted to 24.49 wt%, 39.35 wt%, 49.32 wt%, 56.47 wt%, and 61.86 wt%, respectively. Similarly, the DFA content in the blends of DFA/LG was set to 23.36 wt%, 37.88 wt%, 47.78 wt%, 54.95 wt%, and 60.39 wt%, respectively.

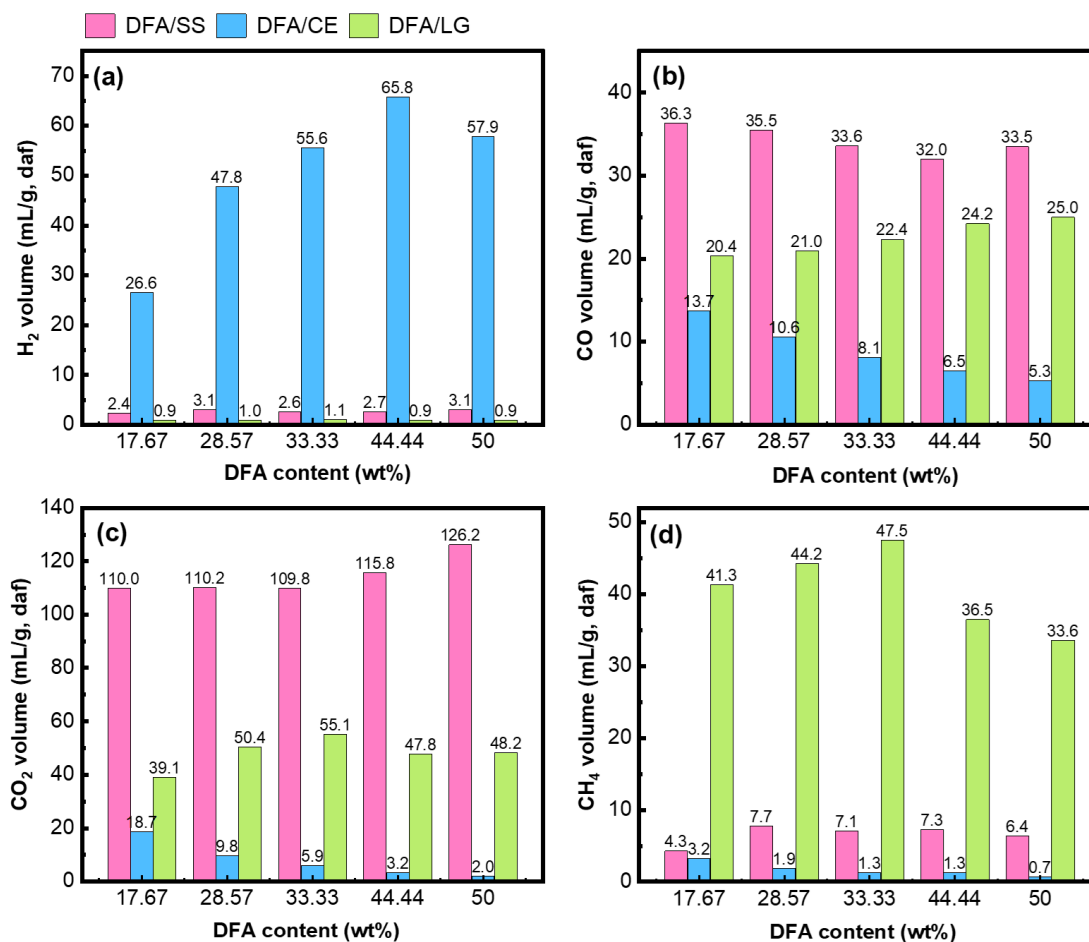


**Fig. 6.** Components resulted in GC analysis of pyrolysis gas: (a) H<sub>2</sub> volume; (b) CO volume; (c) CO<sub>2</sub> volume; (d) CH<sub>4</sub> volume

As depicted in Fig. 6(a), the order of H<sub>2</sub> production was DFA/CE > DFA/SS > DFA/LG, with the H<sub>2</sub> volume from the pyrolysis of DFA/CE being much higher than that from DFA/SS and DFA/LG. Additionally, as the content of DFA in the DFA/CE mixture increased, the H<sub>2</sub> volume first increased and then decreased. This suggests that H<sub>2</sub> was primarily derived from the pyrolysis of cellulose during the pyrolysis. Moreover, DFA promotes H<sub>2</sub> production during the pyrolysis of cellulose. In contrast, in the pyrolysis of DFA/SS, the interaction between cellulose and lignin inhibited H<sub>2</sub> production. As shown in Fig. 6(b), with the increase in the DFA content, the CO volume of DFA/CE gradually decreased, while the CO volume of DFA/LG increased. This indicates that DFA inhibited CO generation from cellulose while promoting the decomposition of lignin to produce CO. Consequently, this effect reduced CO production in the pyrolysis of DFA/SS. As depicted in Fig. 6(c), the CO<sub>2</sub> volume from the pyrolysis of DFA/CE gradually decreased as the DFA content increased, while the CO<sub>2</sub> volume from DFA/LG first increased and then decreased. This indicates that DFA had an inhibitory effect on the decomposition of CE to generate CO<sub>2</sub>. Moreover, the combined CO<sub>2</sub> volume from DFA/CE and DFA/LG was much lower than that from DFA/SS, suggesting that the interaction between cellulose and lignin inherent in the pyrolysis process of DFA/SS greatly promoted the generation of CO<sub>2</sub>. Figure 6(d) presents an analysis of CH<sub>4</sub> volume in pyrolysis gas. It can be observed that the CH<sub>4</sub> volume from the pyrolysis of DFA/LG was higher than that from DFA/SS and DFA/CE. It suggests that the CH<sub>4</sub> in the DFA/SS pyrolysis gas primarily originated from the pyrolysis of lignin within SS. Furthermore, the interaction between lignin and cellulose markedly reduced the CH<sub>4</sub> content in the DFA/SS pyrolysis gas.

## CONCLUSIONS

1. The biomass pyrolysis was remarkably improved by the addition of desulfurization fly ash (DFA), with an optimal content of 33.3 wt% resulting in a notable 5.98% increase in pyrolysis gas volume compared to soybean straw (SS) pyrolysis alone. This finding underscores the potential of DFA as a cost-effective catalyst in biomass conversion processes.
2. The study demonstrated that DFA not only augmented the production of CH<sub>4</sub> and H<sub>2</sub> but it also mitigated CO emissions, resulting in pyrolysis gas with a higher lower heating value. Notably, the H<sub>2</sub> volume was 1.75 times greater than that from SS pyrolysis when 37.5 wt% DFA was employed. These findings help with the efficient exploitation of biomass as a sustainable energy resource.
3. Moreover, the pyrolysis of DFA/CE yielded higher H<sub>2</sub> and lower CO<sub>2</sub>, in contrast to DFA/LG, which tended to produce more CH<sub>4</sub>. The cellulose-lignin interaction in DFA/SS suppressed H<sub>2</sub> production, enhanced CO<sub>2</sub>, and diminished CH<sub>4</sub>, highlighting the crucial role of biomass composition in dictating pyrolysis product selectivity. The mechanistic understanding garnered from this research lays a foundation for the advancement and optimization of biomass gasification processes, leveraging DFA as a catalyst.

## ACKNOWLEDGEMENTS

The work was supported by the National Key Research and Development Program of China (No. 2022YFE0208100), and the Scientific Research Projects of Liaoning province Department of Education (No. LJKZZ20220044).

## REFERENCES CITED

- ASTM D 4006-11. (2012). "Standard test method for water in crude oil by distillation," *Annual Book of Standards*, section 5, Textiles, ASTM, West Conshohocken, PA.
- Bassilakis, R., Carangelo, R. M., and Wójtowicz, M. A. (2001). "TG-FTIR analysis of biomass pyrolysis," *Fuel* 80(12), 1765-1786. DOI: 10.1016/S0016-2361(01)00061-8
- Chen, T. M., Kuschner, W. G., Gokhale, J., and Shofer, S. (2007). "Outdoor air pollution: Nitrogen dioxide, sulfur dioxide, and carbon monoxide health effects," *The American Journal of the Medical Sciences* 333(4), 249-256. DOI: 10.1097/MAJ.0b013e31803b900f
- Díez, D., Urueña, A., Piñero, R., Barrio, A., and Tamminen, T. (2020). "Determination of hemicellulose, cellulose, and lignin content in different types of biomasses by thermogravimetric analysis and pseudocomponent kinetic model (TGA-PKM Method)," *Processes* 8(9), article 1048. DOI: 10.3390/pr8091048
- Li, H., Zhang, H., Li, L., Ren, Q., Yang, X., Jiang, Z., and Zhang, Z. (2019). "Utilization of low-quality desulfurized ash from semi-dry flue gas desulfurization by mixing with hemihydrate gypsum," *Fuel* 255, article ID 115783. DOI: 10.1016/j.fuel.2019.115783
- Li, X. H. J., Dou, Z., and Zhang, T. (2022). "Summary of research progress on industrial flue gas desulfurization technology," *Separation and Purification Technology* 281, article ID 119849. DOI: 10.1016/j.seppur.2021.119849
- Ma, Y., Nie, Q., Xiao, R., Hu, W., and Han, B. (2020). "Experimental investigation of utilizing waste flue gas desulfurized gypsum as backfill materials," *Construction and Building Materials* 245, article ID 118393. DOI: 10.1016/j.conbuildmat.2020.118393
- Mariyam, S., Alherbawi, M., Al-Ansari, T., and McKya, G. (2024). "Upgrading co-pyrolysis products from ternary biomass: An investigative study of commercial and locally-made catalysts," *Biomass and Bioenergy* 191, article ID 107471. DOI: 10.1016/j.biombioe.2024.107471
- Mlonka-Mędrala, A., Evangelopoulos, P., Sieradzka, M., Zajemska, M., and Magdziarz, A. (2021). "Pyrolysis of agricultural waste biomass towards production of gas fuel and high-quality char: Experimental and numerical investigations," *Fuel* 296, article ID 120611. DOI: 10.1016/j.fuel.2021.120611
- Mohan, I., Panda, A., Volli, V., and Kumar, S. (2024). "An insight on upgrading of biomass pyrolysis products and utilization: Current status and future prospect of biomass in India," *Biomass Conversion and Biorefinery* 14, 6185-6203. DOI: 10.1007/s13399-022-02833-2
- Ning, H., Tang, R., Li, C., Gu, X., and Gong, Z. (2025). "Recent advances in process and materials for dry desulfurization of industrial flue gas: An overview," *Separation and Purification Technology* 353, article ID 128425. DOI: 10.1016/j.seppur.2024.128425
- Peng, X., Su, Y., Guo, H., and Guo, J. (2024). "A novel dual-region reduction-oxidation strategy to recover CaO from desulfurization ash," *Fuel* 367, article ID 131202. DOI: 10.1016/j.fuel.2024.131202

- Ren, S., Lei, H., Wang, L., Bu, Q., Chen, S., Wu, J., Julson, J., and Ruan, R. (2013). "The effects of torrefaction on compositions of bio-oil and pyrolysis gas from biomass pyrolysis by microwave heating," *Bioresource Technology* 135, 659-664. DOI: 10.1016/j.biortech.2012.06.091
- Ruan, S., Liu, L., Zhu, M., Shao, C., Xie, L., and Hou, D. (2023). "Application of desulfurization gypsum as activator for modified magnesium slag-fly ash cemented paste backfill material," *Science of The Total Environment* 869, article ID 161631. DOI: 10.1016/j.scitotenv.2023.161631
- She, H., Lv, P., Song, X., Bai, Y., Wang, J., Su, W., Wei, J., Bao, W., and Yu, G. (2024). "Evolution characteristics and mechanism of products from large-particle biomass pyrolysis in molten salt media," *Industrial Crops and Products* 222, article ID 119963. DOI: 10.1016/j.indcrop.2024.119963
- Sun, S., Liu, Z., Xu, Z. J., and Wu, T. (2024). "Opportunities and challenges in biomass electrocatalysis and valorization," *Applied Catalysis B: Environment and Energy* 358, article ID 124404. DOI: 10.1016/j.apcatb.2024.124404
- Tang, C., Zhang, D., and Lu, X. (2015). "Improving the yield and quality of tar during co-pyrolysis of coal and cotton stalk," *BioResources* 10(4), 7667-7680. DOI: 10.15376/biores.10.4.7667-7680
- Wang, R., Feng, Y., Li, K., and Yan, Y. (2024). "Towards the sustainable production of biomass-derived materials with smart functionality: A tutorial review," *Green Chemistry* 26, 9075-9103. DOI: 10.1039/D4GC01771D
- Wang, Y., Wang, Z., Liang, F., Jing, X., and Feng, W. (2021). "Application of flue gas desulfurization gypsum improves multiple functions of saline-sodic soils across China," *Chemosphere* 277, article ID 130345. DOI: 10.1016/j.chemosphere.2021.130345
- Xie, Q., Kong, S., Liu, Y., and Zeng, H. (2012). "Syngas production by two-stage method of biomass catalytic pyrolysis and gasification," *Bioresource Technology* 110, 603-609. DOI: 10.1016/j.biortech.2012.01.028
- Yao, Q., Sun, M., Gao, J., Wang, R., Zhang, Y., Xu, L., and Ma, X. (2019). "Organic sulfur compositions and distributions of tars from the pyrolysis of solvent pretreatment vitrinite of high sulfur coal," *Journal of Analytical and Applied Pyrolysis* 139, 291-300. DOI: 10.1016/j.jaap.2019.03.002
- Zhang, J., Gu, J., Shan, R., Yuan, H., and Chen, Y. (2025). "Advances in thermochemical valorization of biomass towards carbon neutrality," *Resources, Conservation and Recycling* 212, article ID 107905. DOI: 10.1016/j.resconrec.2024.107905
- Zhang, Y., Wang, J., Luo, Q., Yang, Y., Lv, P., Su, W., Bai, Y., Song, X., and Yu, G. (2024). "Intrinsic promotion mechanism of calcium oxide on ketone production during catalytic fast pyrolysis of biomass via experiment and density functional theory simulation," *Bioresource Technology* 410, article ID 131310. DOI: 10.1016/j.biortech.2024.131310
- Zhou, S., Song, J., Tang, C., and Wang, Y. (2024). "Removing residual chlorine in water using carbon-based material derived from co-pyrolysis of cotton stalk and desulfurized ash," *Industrial Crops & Products* 212, article ID 118372. DOI: 10.1016/j.indcrop.2024.118372

Article submitted: November 27, 2024; Peer review completed: December 28, 2024;  
Revised version received and accepted: January 5, 2025; Published: February 10, 2025.  
DOI: 10.15376/biores.20.2.2544-2555